Inorganic Chemistry
Cite This: Inorg. Chem. 2018, 57, 8923−8932
Article
pubs.acs.org/IC

Oxidative Release of Copper from Pharmacologic Copper Bis(thiosemicarbazonato) Compounds

John J. Sirois,[†,⊥] Lillian Padgitt-Cobb,[‡] Marissa A. Gallegos,[†] Joseph S. Beckman,[‡,§] Christopher M. Beaudry,[†] and James K. Hurst*[,‡]

[†]Department of Chemistry, [‡]Department of Biochemistry & Biophysics, [§]Linus Pauling Institute, Oregon State University, Corvallis, Oregon 97331-7305, United States

Supporting Information

ABSTRACT: Intracellular delivery of therapeutic or analytic copper from copper bis-thiosemicabazonato complexes is generally described in terms of mechanisms involving one-electron reduction to the Cu(I) analogue by endogenous reductants, thereby rendering the metal ion labile and less strongly coordinating to the bis-thiosemicarbazone (btsc) ligand. However, electrochemical and spectroscopic studies described herein indicate that one-electron oxidation of Cu^{II}(btsc) and Zn^{II}ATSM (btsc = diacetyl-bis(4-methylthiosemicarbazonato)) complexes occurs within the range of physiological oxidants, leading to the likelihood that unrecognized oxidative pathways for copper release also exist. Oxidations of Cu^{II}(btsc) by H_2O_2 catalyzed by either myeloperoxidase or horseradish peroxidase, by HOCl and taurine chloramine (which are chlorinating agents generated primarily in activated neutrophils from MPO-catalyzed reactions), and by peroxynitrite species (ONOOH, $ONOOCO_2^-$) that can form under certain conditions of oxidative stress are demonstrated. Unlike reduction, the oxidative reactions proceed by irreversible ligand oxidation, culminating in release of Cu(II). 2-Pyridylazoresorcinol complexation was used to demonstrate that Cu(II) release by reaction with peroxynitrite species involved rate-limiting homolysis of the peroxy O−O bond to generate secondary oxidizing radicals ($NO_2^{\bullet}$, $^{\bullet}OH$, and $CO_3^{\bullet-}$). Because the potentials for Cu^{II}(btsc) oxidation and reduction are ligand-dependent, varying by as much as 200 mV, it is clearly advantageous in designing therapeutic methodologies for specific treatments to identify the operative Cu-release pathway.

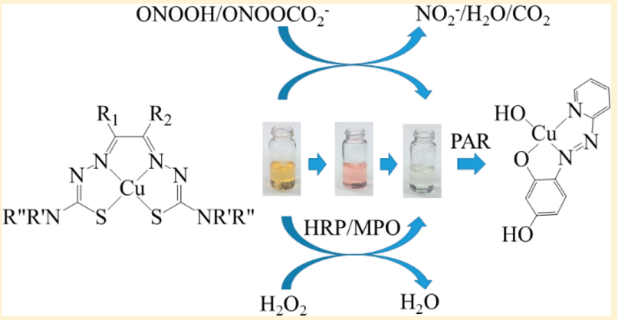

INTRODUCTION

Copper(II) bis-thiosemicarbazonato complexes (Cu^{II}(btsc)) (Chart 1) show promise as radioimaging agents and tissue-specific therapeutic agents for treatment of ailments as diverse as solid cancerous tumors and neurological disorders.[1−4] Based primarily upon the observation that copper accumulates in hypoxic cells to a greater extent than normoxic cells,[1] a model has been advanced that ascribes delivery to the cell interior by passive transmembrane transport of charge-neutral Cu^{II}(btsc), followed by intracellular reduction to Cu(I) and its release and sequestration at biological copper-binding sites (e.g., reductive pathway, Scheme 1).[1,5] The one-electron reduction potentials for Cu^{II}(btsc) complexes are low (see below), however, with E° = −0.23 to −0.47 V (in DMSO vs NHE) being estimated by cyclic voltammetry, so that efficient Cu(II) reduction in these complexes should be thermodynamically limited to highly reducing biological systems. Correspondingly, the low-potential redox sites in several NADH or NADPH-dependent electron transport chains have been shown to be capable of reducing Cu^{II}(btsc) complexes,[5−7] whereas weaker biological reductants such as ascorbate and biological thiols are much less effective, and reactivity is observed only in instances where the medium contains strongly complexing Cu(I) ligands that can drive the reactions forward.[8] An almost overlooked feature of these Cu^{II}(btsc) complexes is that they can also be oxidized at potentials that are well within the range of biological oxidants (~0.81−0.94 V in DMSO vs NHE); see below). We demonstrate herein that oxidations by peroxidase-catalyzed H_2O_2, biological chlorinating agents, or peroxynitrite-derived radicals lead to rapid oxidative degradation of the btsc ligand with concomitant release of Cu(II) (e.g., oxidative pathway, Scheme 1).

Chart 1. Generic Chemical Structure of Cu^{II}(btsc) Compounds

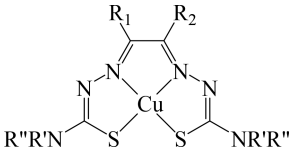

Received: March 29, 2018
Published: July 6, 2018

DOI: 10.1021/acs.inorgchem.8b00853
Inorg. Chem. 2018, 57, 8923−8932

Scheme 1. Proposed Reductive and Oxidative Pathways for Intracellular Delivery of Cu from CuATSM[a]

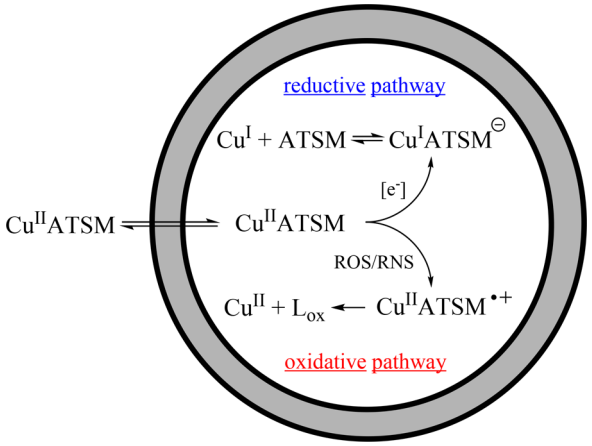

[a]ROS/RNS = cellularly generated reactive oxidative species and reactive nitrosative species, respectively.

RESULTS AND DISCUSSION

Electrochemistry. The electrochemical redox properties of the btsc free ligands and metal ion complexes are illustrated in the cyclic voltammograms for ATSM (diacetyl-bis(N^4-methylthiosemicarbazone) (R_1, R_2, R′ = CH_3, R″ = H) shown in Figure 1. Massive irreversible degradation of

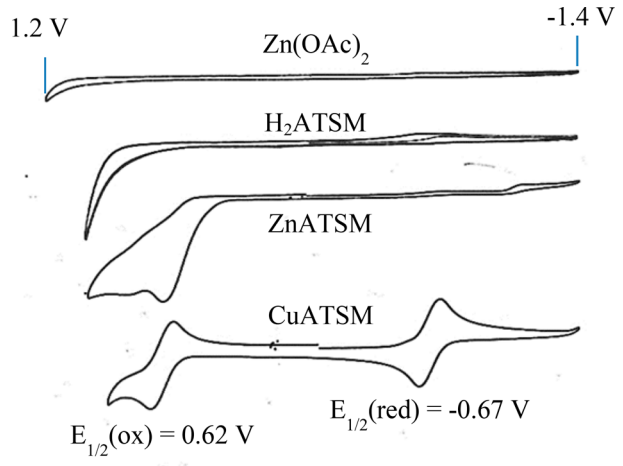

Figure 1. Cyclic voltammograms of 5 mM H_2ATSM, ZnATSM, and CuATSM in DMSO vs Ag/AgCl.

uncoordinated H_2ATSM began at ~0.9 V (vs Ag/AgCl); binding of either redox-active Cu(II) or redox-inactive Zn(II) ions introduced a new oxidation peak at ~0.6 V. For ZnATSM, this was closely followed by additional irreversible oxidation processes, and a corresponding reduction half-wave was not observed. For CuATSM, oxidation was quasi-reversible; repetitive cycling through the oxidation wave led to the appearance of new reduction peaks at ~0 to −0.2 V, suggestive of accumulation of degradation products (not shown). This behavior is consistent with earlier accounts of the inability to isolate stable oxidized species from constant potential electrolysis.[9] A quasi-reversible reduction wave was also seen at −0.67 V in the CuATSM voltammogram; because the ZnATSM voltammogram was devoid of reduction waves, it can be unambiguously assigned as the metal-centered Cu(II) → Cu(I) reduction. From the relative amplitudes of the oxidation and reduction waves exhibited by CuATSM, which are nearly equal, it follows that the oxidation process is also a one-electron event. Analogous electrochemical behavior was observed for an additional 18 Cu^{II}(btsc) and Zn^{II}(btsc) complexes which differed in the identities of alkyl and aromatic substituents in the R_1 and R_2 positions, as well as the extent of alkylation on R′ and R″ (Chart 1). The oxidation and reduction half-wave potentials measured for the Cu^{II}(btsc) analogues are given in Figure 2 as an electrochemical series,

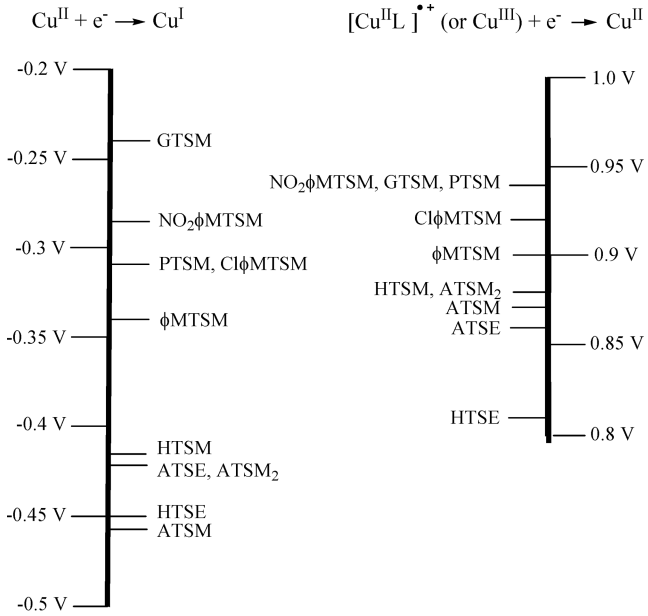

Complex	R_1	R_2	R'	R"
GTSM:	H	H	H	Me
PTSM:	H	Me	H	Me
ATSM:	Me	Me	H	Me
ATSE:	Me	Me	H	Et
$ATSM_2$:	Me	Me	Me	Me
HTSM:	Et	Et	H	Me
HTSE:	Et	Et	H	Et
φMTSM:	φ	Me	H	Me
ClφMTSM:	4-Clφ	Me	H	Me
NO_2φMTSM:	4-NO_2φ	Me	H	Me

Figure 2. Electrochemical series for representative Cu^{II}(btsc) complexes in DMSO (this work). Reduction potentials estimated from cyclic voltammetry from $E_{1/2}$ values using $Fc^{+/o}$ as an internal standard and referenced to NHE by assuming $E°(Fc^{+/o})$ = 680 mV vs NHE.[11] Specific ligands are designated according to the key, where substituent positions are identified in Chart 1 (Me = CH_3; Et = CH_3CH_2; ϕ = C_6H_5).

where the experimental potentials measured against an Ag/AgCl reference electrode were adjusted to NHE as indicated in the figure caption. The oxidation and reduction $E_{1/2}$ values obtained varied from 0.81 to 0.94 V and −(0.23−0.46) V (vs NHE), respectively, over the series. Oxidation of ZnATSM must be ligand-centered, giving rise to a ligand radical cation, i.e., [Zn^{II}-ATSM$^•$]$^+$, as the initial one-electron oxidized species. Given that CuATSM is oxidized at essentially the same potential (Figure 1), the ligand may also be the reaction site in this complex. However, the Cu^{II}(btsc) complexes possess structural features (anionic strong donor and highly polarizable

DOI: 10.1021/acs.inorgchem.8b00853
Inorg. Chem. 2018, 57, 8923−8932

lead-in atoms in a tetradentate square planar geometry) that would stabilize the d^8 Cu(III) center and could thereby lower its reduction potential into the observed range. Numerous similarly structured cupric complexes have in fact been described for which $E°(Cu^{III/II}) \sim 0.7-0.9$ V (NHE).[10] The experiments described herein do not allow discrimination between metal-centered and ligand-centered oxidation of Cu^{II}(btsc), although one might speculate that the greater stability of its oxidized state evident in the CuATSM and ZnATSM voltammograms (Figure 1) relates to its capacity to undergo metal-centered oxidation.

Chemical Oxidations: General Considerations. The optical properties of btsc compounds are well-suited for spectrochemical analysis, exhibiting intense, clearly resolved absorption bands for the free ligand and its Cu(II) and Zn(II) complexes; typical spectra (for ATSM) are shown in Figure 3a.

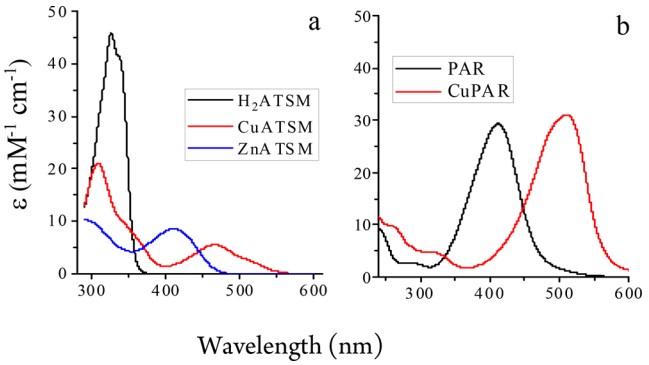

Figure 3. Optical spectra. Panel a: H_2ATSM and its complexes in 20 mM MOPS, pH 7.2, plus 50 mM SDS; panel b: PAR and CuPAR in 50 mM phosphate, pH 7.2, plus 20 mM SDS.

To study oxidative reactions, we generally used 3-(*N*-morpholino)propanesulfonic acid (MOPS) or phosphate-buffered media containing sodium dodecyl sulfate (SDS) at concentrations above its critical micelle concentration;[12] the presence of micelles promoted solubilization of the btsc compounds while allowing use of aqueous oxidant systems. The micellar environment also provides a hydrophobic microphase which may mimic the actual internal locus of Cu^{II}(btsc) compounds adsorbed by cells; specifically, recent confocal fluorescence microscopic studies using BODIPY-tagged Cu^{II}ATSM have suggested that the compound resides predominantly within intracellular lipid droplets and the membrane ultrastructure of cells.[13]

Peroxidase-Catalyzed Oxidation by Hydrogen Peroxide. CuATSM is unreactive toward H_2O_2 (Figures 4 and S1). However, when a peroxidase was introduced to solutions containing CuATSM or ZnATSM and H_2O_2, rapid decolorization occurred over the entire optical spectrum, indicating that the complex had been oxidatively degraded. These reactions were demonstrated for both myeloperoxidase (MPO)[14] ($E_7°'(compound^{I}/compound^{II})$ = 1.35 V; $E_7°'(compound^{II}/Fe^{III}$-MPO) = 0.97 V) (Figure 3), and the less strongly oxidizing horseradish peroxidase (HRP)[15] ($E_7°'(compound^{I}/compound^{II})$ = 0.92 V; $E_7°'(compound^{II}/Fe^{III}$–HRP) = 0.94 V) (Figure S1). Based upon their one-electron reduction potentials, compounds I and II of both peroxidases are themodynamically competent to drive oxidation of Cu^{II}(btsc) and Zn^{II}(btsc) ligands. All components of the enzymatic systems were required for reaction to occur, and the order of

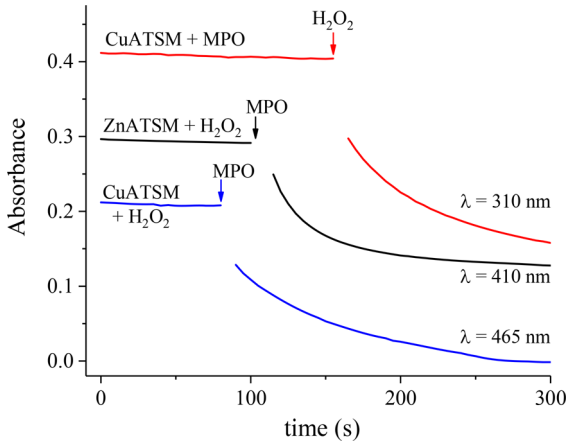

Figure 4. Representative kinetic traces for MPO/H_2O_2/M-ATSM reactions. Conditions: 0.020 mM CuATSM, 0.10 mM H_2O_2, 55 nM MPO (red); 0.020 mM ZnATSM, 0.10 mM H_2O_2, 37 nM MPO (black); 0.030 mM CuATSM, 0.10 mM H_2O_2, 110 nM MPO (blue). In 5 mM MOPS, pH7.2, at 23 °C. Absorbances of the lower two traces have been offset to allow simultaneous display; also, for CuATSM, absorbance shown at 465 nm is 3× actual value.

addition of H_2O_2 and MPO or HRP was immaterial to the catalytic reaction rates. The reactions were unaffected by inclusion of 1 mM DTPA to scavenge adventitious metal ions, but were partially inhibited when 0.1–3.0 mM of the heme peroxidase inhibitor, NaN_3, was added to the medium. Irreversible enzyme inactivation also accompanied turnover; typically, standard guaiacol assays indicated that ~50% MPO activity was lost following catalysis of CuATSM degradation under these conditions. Copper release was probed using 4-(2-pyridylazo)resorcinol (PAR), which under the experimental conditions rapidly coordinates Cu(II) (Figure S2) to form a tightly bound terdentate 1:1 complex[16] (Figure S3, TOC graphic) possessing a strong visible absorption band (λ_{max} = 511 nm, ε_{511} = 28 mM^{-1} cm^{-1}) (Figure 3b). Transmetalation from CuATSM to PAR does not occur under these conditions (Figure S4). Because the ε-value for CuPAR at its absorption maximum is ~6-fold greater than that for CuATSM (Figure 3), it is easy to detect free Cu(II) in the presence of CuATSM from spectral changes accompanying addition of PAR. Cu(II) release from the CuATSM/MPO/H_2O_2 reaction was demonstrated in this fashion by adding PAR to the product solution, upon which formation of CuPAR corresponding to ~40% of the CuATSM originally present was calculated from the spectral changes (Figure S5). These data set a conservative lower limit on MPO turnover of 100-fold under the experimental conditions of Figure 4. Unlike its metal complexes, the H_2ATSM free ligand was unreactive in the presence of HRP/H_2O_2 (Figure S1), consistent with thermodynamic expectations.

The capacity of these compounds to modulate the reactivity of HRP under standard assay conditions using 2,2′-azino-bis(3-ethylbenzothiazoline-6-sulfonic acid) (ABTS) as a one-electron donor[17] was also briefly examined. As shown in Figure 5, addition of CuATSM increased the initial velocity of the HRP-catalyzed H_2O_2 oxidation product ($ABTS^{\bullet+}$) in a dose-dependent manner, accelerating the reaction by ~3.5-fold at the highest concentrations used. This unexpected result suggests that the complex can mediate electron transfer between ABTS and HRP compounds I and II via its own one-electron oxidized state. In contrast, addition of ZnATSM

DOI: 10.1021/acs.inorgchem.8b00853
Inorg. Chem. 2018, 57, 8923–8932

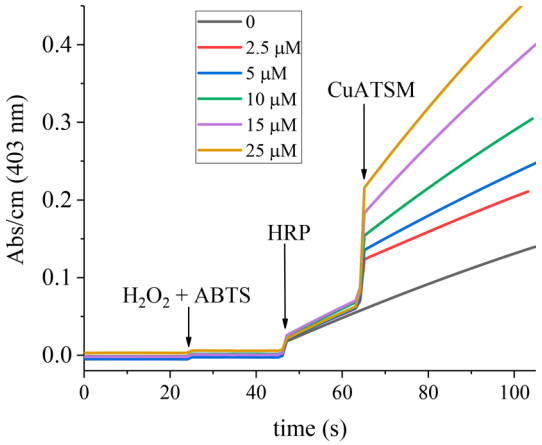

Figure 5. CuATSM acceleration of HRP-catalyzed oxidation of ABTS by H_2O_2 under steady-state conditions. CuATSM added at the indicated concentrations to 50 μM H_2O_2, 50 μM ABTS, and 4 nM HRP in 10 mM phosphate, pH 7.2, at 23 °C. The order of addition of reactants and catalysts is indicated by the vertical arrows. Apparent discontinuities in the kinetic traces at the points of addition are artifactual and arise because it was necessary to briefly stop recording the data to manually add reagents. Thus, spectral changes occurring during these intervals are not recorded, but appear as instantaneous "jumps" once the kinetic traces are restarted.

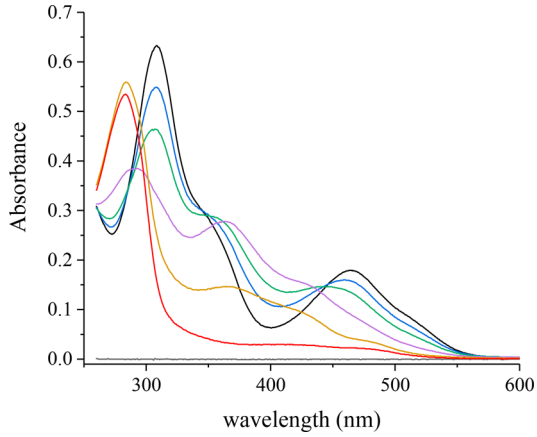

Figure 6. Oxidation of CuATSM by HOCl. Spectra are for 30 μM CuATSM in 20 mM phosphate, pH 7.2, plus 25 mM SDS (black) and product solutions obtained following addition of 30 μM (blue), 60 μM (green), 120 μM (purple), 195 μM (orange), and 240 μM (red) HOCl.

or, to a lesser extent, free H_2ATSM to the assay medium led to reduction in the initial rates of $ABTS^{\bullet+}$ formation under otherwise identical reaction conditions (Figures S6 and S7). Accordingly, neither oxidized ZnATSM nor H_2ATSM appear capable of reacting with ABTS. These reactivity differences are consistent with the electrochemical redox behavior displayed in Figure 1, where CuATSM oxidation was fully reversible on a voltammetric sweep time scale comprising several seconds, but degradation of the other species was too rapid to permit re-reduction of the initially oxidized forms, leading to irreversible voltammetric peaks.

Oxidation by Chlorinating Agents. Hypochlorous acid is widely regarded as a primary MPO-generated component of mammalian cellular defense systems against invading pathogens.[18] The prospect therefore exists that HOCl, as well as secondary chlorinating agents such as chloramines formed by its reaction with physiological amines and amino acids, could promote release of Cu from Cu^{II}(btsc) complexes at sites of infection where phagocytes are activated. Indeed, we found that HOCl and taurine chloramine (*N*-chloro-2-aminoethanesulfonate) oxidatively degrade CuATSM under conditions that mimic the physiological milieu. Shown in Figure 6 are spectral changes accompanying incremental additions of HOCl to CuATSM in an aqueous micellar medium. One observes initially a progressive hypsochromic shift of the visible band with decreasing absorbance in the UV band, followed at higher oxidant levels a hypsochromic shift in all bands accompanied by the appearance and subsequent decline of new bands in the near-UV region. These changes, together with the absence of any isosbestic points, indicate that multiple products are formed over the course of the titration. Complete bleaching of the CuATSM spectrum requires addition of ~10-fold molar excess (~20 oxidizing equivalents) HOCl. The reactions are complete within the time of mixing of reactant solutions. Preliminary stopped-flow studies suggest that the initial reaction step has a bimolecular rate constant of $\sim 2 \times 10^7$ M^{-1} s^{-1} under these conditions. Very similar spectral changes were seen when taurine chloramine was used in place of HOCl (Figure S8), although the reactions in this case were considerably slower, requiring nearly an hour following chloramine addition to reach completion. This dynamic behavior is consistent with the much lower intrinsic reactivity of primary chloramines relative to HOCl. Release of Cu(II) at various points in the titration was probed by adding PAR to the solution and determining the extent of CuPAR formation. From these studies, it was evident that free Cu(II) appeared very early in the course of the titration, e.g., after addition of one molar equivalent HOCl, the CuPAR formed was 16%, and after addition of two equivalent, it was 29% of the CuATSM initially present (Figure S9).

Peroxynitrite Reactions. The peroxynitrite anion ($ONOO^-$) is formed via radical coupling in tissues that are simultaneously generating superoxide anion ($O_2^{\bullet-}$) (e.g., as a byproduct of respiratory electron transport or via phagocyte NADPH oxidases) and nitric oxide (NO) (e.g., by aerobic oxidation of L-arginine catalyzed by constitutive or inducible forms of nitric oxide synthetase).[19,20] In the absence of oxidizable substrates, the anion is relatively stable, but addition of Lewis acids (H^+, CO_2, metal ions) to the terminal oxygen weakens the peroxo O−O bond, giving rise to net decomposition to O_2 and NO_2^- and/or isomerization to nitrate.[21−23] Decomposition occurs via homolysis of the peroxo O−O bond, leading to formation of inorganic radicals ($OH^{\bullet}$, $CO_3^{\bullet-}$, and $NO_2^{\bullet}$),[21,22] which are powerful one-electron oxidants.[24] Oxidations by peroxynitrite can therefore be complex, involving either direct bimolecular reaction of the reductant with ONOOH (or, less frequently, $ONOO^-$) or indirect reactions involving the secondary radicals formed during peroxynitrite decomposition.[25] These two pathways can easily be distinguished from the kinetic patterns of the oxidative reactions, which for the direct pathway is simple mixed-second order and for the indirect pathway is first-order in peroxynitrite and zero-order in reductant concentration. Moreover, in the indirect pathway, the oxidation rate constant coincides with the peroxynitrite decomposition rate constant under the prevailing conditions, and maximal product yields are ≤30% of stoichiometric, reflecting the minor fraction of radicals that escape recombination within the solvent cage to give the isomerized oxidant, i.e., NO_3^-.[23,25] As described

DOI: 10.1021/acs.inorgchem.8b00853
Inorg. Chem. 2018, 57, 8923−8932

below, all of the Cu^{II}(btsc) complexes examined reacted with peroxynitrite via the indirect pathway. Additionally, for those complexes that are relatively easily oxidized, evidence for a competing direct reaction between ONOOH and the complexes was found.

Peroxynitrous acid (ONOOH) and the peroxynitrite-CO_2 adduct ($ONOOCO_2^-$) rapidly degraded ZnATSM and Cu^{II}(btsc) complexes (including CuATSM and analogues for which R_1, R_2 = H (CuGTSM) or R_1 = C_6H_5, R_2 = CH_3 (CuϕMTSM)). Stopped-flow spectrophotometric analyses established the following properties of the reactions: (1) the oxidation pathway involved first-order reactions whose rate constants were pH-dependent and nearly identical to independently measured constants for pH-dependent peroxynitrite decomposition (Table 1, Group A);[22] (2) similarly,

Table 1. Comparison of Experimentally Determined (k_d) and Calculated (k_{calc}) First-order Rate Constants for Peroxynitrite Decomposition with Oxidation (A–C and E) and Cu(II) Release (D) from Cu^{II}(btsc) Complexes (k^{ox})[a]

	k_{ox} (s^{-1})	k_d (s^{-1})	k_{calc} (s^{-1})[b]
A. CuATSM + ONOOH → products			
pH 6.3	0.30–0.67		0.58
pH 7.4	0.22–0.23	0.19[c]	0.11
pH 9.8	very slow		0.0006
B. CuATSM + $ONOOCO_2^-$ → products[d]			
pH 7.5	9.1–10.5	29[c]	9.1
C. CuGTSM + ONOOH → products			
pH 7.4	0.25–0.40	0.19	0.11
D. CuATSM + ONOOH + PAR → CuPAR + other products			
pH 7.4	0.20	0.19	0.11
E. PAR + ONOOH → products			
pH 7.3	0.23		0.16

[a]In 25 mM phosphate, 25 mM SDS, 23 °C, except where noted. [b]Ref 22. [c]SDS absent. [d]Medium contained 12.5 mM total carbonate (as CO_2 + HCO_3^-).

decomposition and CuATSM oxidation rate constants were accelerated by equal amounts in the presence of CO_2 (Table 1, Group B); and (3) the rate constants for Cu^{II}(btsc) oxidation were independent of the identity of the complex (cf. Table 1, Groups A (CuATSM) and C (CuGTSM)); (4) when PAR was present in the reaction solutions, the rate constant for CuPAR formation was also first-order and equal to that for peroxynitrite decomposition (Figure 7; Table 1, Group D). Independent measurements established that Cu(II)-PAR association rates are considerably more rapid than the redox reactions under investigation (Figure S2), that free PAR reacts only with the peroxynitrite-generated radicals (Table 1, Group E, Figure S9), and that CuPAR is unreactive toward all of the peroxynitrite-derived oxidants. This set of circumstances, including the previously mentioned absence of Cu^{II}(btsm) → Cu^{II}PAR transmetalation, allow one to conclude that Cu(II) release occurs by reaction of CuATSM with the secondary radicals and not from direct bimolecular reaction between CuATSM and peroxynitrite species. Overall, these reactions exhibit the characteristics of indirect reactions of peroxynitrite for which the actual oxidants are $NO_2^\bullet$ and $OH^\bullet$ or $CO_3^{\bullet-}$ formed by rate-limiting homolysis of the ONOOH or $ONOOCO_2^-$ O–O bonds.[21]

Titrimetric addition indicated that a ~14-fold excess of peroxynitrite over CuATSM was required to achieve complete

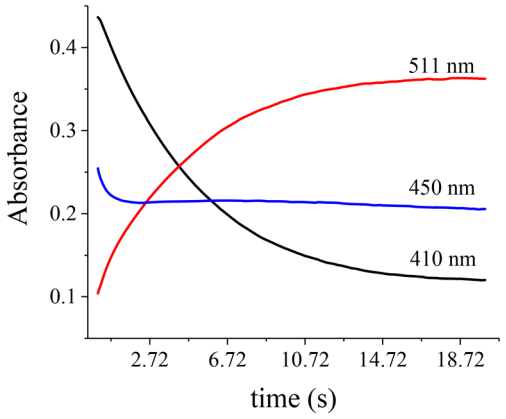

Figure 7. Kinetic traces at selected wavelengths of the reaction of CuATSM with peroxynitrite in the presence of PAR. Conditions: 0.020 mM CuATSM, 0.25 mM ONOOH, and 0.015 mM PAR in 25 mM phosphate (final pH 7.44) plus 50 mM SDS, 23 °C. CuPAR formation at 511 nm (red); PAR consumption at 410 nm (black); CuPAR/PAR isosbestic point at 450 nm (blue). Reactions at 511 and 410 nm are first-order with identical k = 0.20 s^{-1}; for comparison, independently measured first-order peroxynitrite decay under the same conditions gives k_d = 0.19 s^{-1}. The reaction at 450 nm can be attributed to CuATSM + ONOOH, which shows a characteristic fast component corresponding to direct reaction with ONOOH and slower reactions involving decay of oxidized CuATSM (see text for discussion).

bleaching of the complex in neutral solutions. At this point, ~70% of the Cu(II) present was released and could be recovered as CuPAR upon addition of PAR to the product solution. Peroxynitrite involvement was confirmed by control studies in which ONOOH was allowed to decompose to nitrate and nitrite/O_2 for several minutes prior to addition to CuATSM-containing solutions;[22] under these conditions, no reaction was observed. Assuming that this reaction is carried by generation of inorganic radicals derived from O–O bond homolysis, this corresponds maximally to about 8 oxidizing equivalents (i.e., 4 ONOOH molecules) per complex. Clearly, then, the reaction is a multistep oxidation process. Intermediate species were not spectrally detected during the redox titration. Spectral bandshapes and peak maxima (308 and 462 nm) remained unchanged over the course of the titration, with absorbency changes that corresponded linearly to the amount of added oxidant. However, a transiently generated red intermediate that slowly faded within several seconds was visually apparent following bolus addition of ONOOH to CuATSM (Figure 8). Stopped-flow kinetic analysis with ONOOH in 10-fold excess indicated that formation of the red intermediate was faster than peroxynitrite decomposition (Figure 8) and therefore must involve direct bimolecular reaction of ONOOH with CuATSM. Intermediate decay occurred on time scales that approximated those for peroxynitrite decomposition and may therefore represent reaction between initially formed partially oxidized complexes and peroxynitrite-derived oxidizing radicals (Figure 8). Formation of this transient is apparently not obligatory for net oxidation of Cu^{II}(btsc) complexes, however. No intermediates were detected (either visually or by stopped-flow analysis) when CuGTSM was used in place of CuATSM. A survey of various Cu^{II}(btsc) complexes using visual detection indicated that only the more easily oxidized members of the series (with $E_{1/2}$(ox) ≤ 0.92 V) (Figure 1)) generated red

DOI: 10.1021/acs.inorgchem.8b00853
Inorg. Chem. 2018, 57, 8923–8932

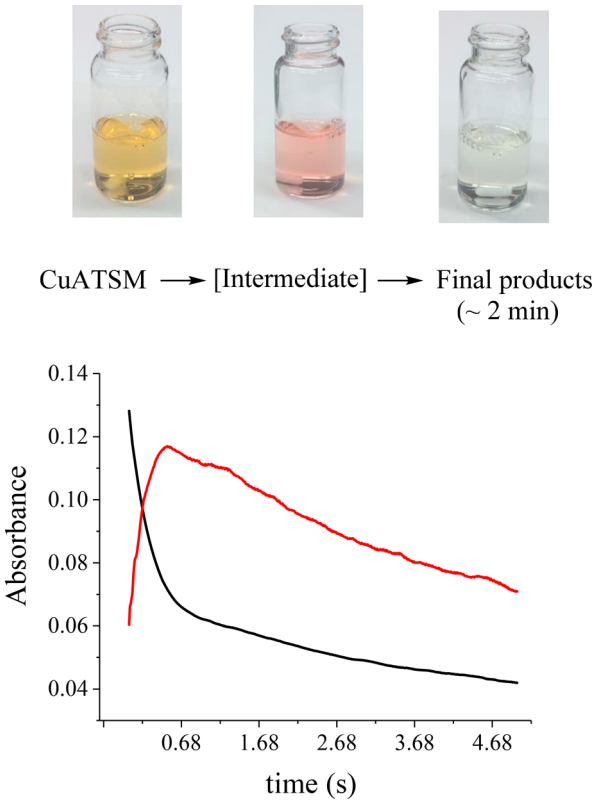

Figure 8. Stopped-flow traces of the CuATSM-ONOOH reaction. Conditions: 0.025 mM CuATSM + 0.25 mM ONOOH in 25 mM SDS plus 25 mM phosphate, pH 7.5, at 23 °C. Overlay of biphasic traces for CuATSM decay at 465 nm (black) and intermediate formation and decay at 590 nm (red, 4× actual absorbance). Photographs above the kinetic traces give a visual record of intermediate formation and decay in the reaction. Conditions: 0.03 mM CuATSM with 0.5 mM peroxynitrite in 50 mM phosphate plus 20 mM SDS, pH 7.2, 23 °C.

intermediates upon exposure to peroxynitrite; moreover, the extent of formation of the CuATSM intermediate was highly pH-dependent, decreasing with decreasing acidity from pH 6.3 to 9.8, where it was barely detectable by stopped-flow analysis. The kinetic waveforms obtained at pH 7.2 were accurately reproduced by fitting to a double exponential form, suggesting that the reactions proceeded by concurrent pathways. Overall, these data are consistent with simultaneous expression of two pathways in which (1) thermodynamically limited direct reaction of the more easily oxidized complexes within the Cu^{II}(btsc) series with ONOOH, but not with the less strongly oxidizing $ONOO^-$ (pK_a = 6.6), runs in parallel with (2) indirect reactions of peroxynitrite-derived oxidizing radicals that can rapidly oxidize all complexes within the series. Finally, transient diode array spectrophotometry of CuATSM indicated that the spectrum of the intermediate has a relatively intense near UV band at 340 nm, and very broad weak absorption above ~500 nm that accounts for the red coloration. These spectral features are consistent with either ligand radical formation (e.g., $Cu^{II}(ATSM)^{\bullet+}$) or oxidation to Cu(III)ATSM. Specifically, strikingly similar spectra have been observed for multidentate Cu(II) and other metal complexes containing phenoxyl and N-heterocyclic ligand radicals,[26,27] but many tetradentate square-planar Cu(III) complexes also exhibit intense LMCT absorption bands in the near-UV region.[10] Stopped-flow analyses also indicated that several intermediates could be temporally resolved in reactions of CuϕMTSM with peroxynitrite and, although ZnATSM was extensively degraded by peroxynitrite, no discrete intermediates could be detected in that reaction.

Biomedical Implications. Mechanisms for intracellular release of copper are yet to be identified. However, it is likely that both reductive and oxidative pathways (Scheme 1) can prevail under different physiological conditions. Thus, for example, the reductive pathway seems well-established in positron-emission tomography (PET) applications to detect hypoxia, where the extent of intracellular copper accumulation parallels the reduction potentials of Cu^{II}(btsc) complexes.[1] In similar PET imaging studies to detect regions of oxidative stress in tissues from patients suffering from neurodegenerative disorders, enhanced copper release has been attributed to increased reducing capacity in cells as a consequence of NADH accumulation caused by impaired mitochondrial electron transport,[28,29] although these conditions also promote formation of reactive oxygen species (ROS) that are thermodynamically competent to oxidize the complexes. Moreover, disease progression in neurological disorders for which Cu^{II}(btsc) treatment may have therapeutic benefit is characterized by oxidative damage by ROS and reactive nitrosative species, the latter possibly including ONOOH. The antineoplastic activity of certain Cu^{II}(btsc) complexes (notably CuGTSM) has recently been attributed to their capacity for intracellular generation of ROS via redox cycling between the Cu(II) and Cu(I) states of the complexes; notably, in these studies, a marked dependence of cellular toxicity upon the $Cu^{II/I}$(btsc) reduction potential was observed.[30] The acceleration of HRP-catalyzed ABTS oxidation by H_2O_2 observed in this study when CuATSM was introduced into the assay medium (Figure 5) suggests that cycling between Cu^{II}(btsc) and oxidized Cu(btsc) states might also occur in biological settings. Biological precedents for this type of reactivity can be found in the reactions of galactose oxidase (GAO), a protein containing a single active site copper atom that catalyzes aerobic oxidation of primary alcohols to the corresponding aldehydes with stoichiometric formation of H_2O_2,[31] and copper complexes that have been developed as functional models of the catalytic reaction center.[26] A pertinent example is the study by Wieghardt and co-workers on the oxidative chemistry of *N*,*N*′-bis(3,5-di-*tert*-butyl-2-hydroxyphenyl)-1,2-phenylenediamine.[32] This ligand forms monomeric tetradentate square-planar complexes with Cu(II) and Zn(II) with N_2O_2 coordination sets that are structurally quite similar to the M^{II}(btsc) complexes studied here. Five different oxidation states are accessible in the GAO model complex; catalytic aerobic oxidation of primary alcohols to aldehydes, i.e., $RCH_2OH + O_2 \rightarrow RCHO + H_2O_2$, is proposed to occur by net two-electron cycling between two ligand radical states of the complexes, namely, a reduced state containing a di(hydroxyphenyl)-diiminosemiquinone ligand and an oxidized state containing a hydroxyphenyl(phenoxyl)-diiminoquinone ligand. Notably, both the Cu(II) and Zn(II) complexes are effective catalysts. Collectively, the studies on GAO catalysis and CuATSM cocatalysis of the HRP/H_2O_2/ABTS reaction suggest a scenario in which intracellular release of copper might occur via a reaction sequence in which transmembrane diffusion of Cu^{II}(btsc) is followed by complex-catalyzed generation of the oxidant (H_2O_2) that leads to its own oxidative destruction. Upregulation of MPO in damaged neuronal tissues has also been documented, opening

DOI: 10.1021/acs.inorgchem.8b00853
Inorg. Chem. 2018, 57, 8923−8932

pathways for formation of additional oxidizing species as part of the neurodegenerative processes.[33−36] In this context, the present studies have clearly demonstrated facile cupric ion release following oxidation by either ONOOH/$ONOOCO_2^-$ or MPO-catalyzed peroxide systems, including HOCl, the physiological product of neutrophil MPO-catalyzed reactions. Our demonstration that reactions of major ROS and RNS oxidants effect efficient Cu(II) release from Cu^{II}(btsc) complexes establish the plausibility of similar reactions occurring in biological tissues, particularly in regions undergoing oxidative stress. Distinguishing between oxidative and reductive pathways in biological environments may prove difficult, but we note that the fate of the btsc ligand is fundamentally different in the two general pathways outlined in Scheme 1, where it remains intact following reduction of the complex to continually cycle metal ions, but is modified with loss of metal-binding capacity in the oxidative pathway. Thus, the pathways could presumably be distinguished in specific instances by quantitative determination of the fate of the ligand. Finally, we note that cupric ion in the presence of H_2O_2 is potently bactericidal.[37] Use of Cu^{II}(btsc) complexes as copper delivery systems offers potential for developing new antibiotics, as has been demonstrated in recent studies.[38,39] Interestingly, one proposed bactericidal mechanism is inhibition of respiration through direct binding of intact Cu^{II}(btsc) to the bacterial electron transport chain. Presumably, for this application, one would seek to identify Cu^{II}(btsc) complexes that underwent minimal intracellular degradation.

EXPERIMENTAL SECTION

Materials. All reagents and solvents used in preparation and characterization of synthetic compounds were purchased through TCI America or Sigma-Aldrich and used directly without purification. Bisthiosemicarbazone ligands used in these studies were prepared following the general procedure outlined below:[30]

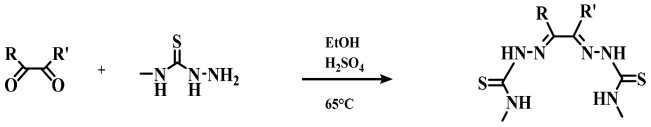

Typically, 2.0 equiv of 4-methyl-thiosemicarbazide was added to an oven-dried 250 mL round-bottom flask containing 50 mL anhydrous EtOH, and the mixture was heated to 65 °C while stirring until the reactant completely dissolved. One equivalent of the appropriate dicarbonyl compound was then added dropwise to the stirring solution, followed by 5 drops of conc H_2SO_4. Within 5 min a precipitate formed; following overnight stirring, the mixture was filtered and sequentially washed with deionized water, MeOH and EtOH. Product analyses included (1) ^{1}H NMR and ^{13}C NMR spectra, recorded in d^6-DMSO on a Bruker 700 MHz Avance III spectrometer and a Bruker 400 MHz DPX-400 spectrometer, respectively and (2) mass spectra acquired on a Thermo LTQ-FT Ultra hybrid linear ion trap-Fourier transform ion cyclotron resonance mass spectrometer with a Finnigan Ion Max API source configured for ESI in positive ion mode. NMR and mass spectra for each compound agreed with those previously reported in the literature.[30] Specifically, for diacetyl-bis(4-methylthiosemicarbazone) (H_2ATSM), ^{1}H NMR (700 MHz, d^6-DMSO): 10.215 (s, 2H), 8.372 (q, 2H, J = 5, J = 13), 3.023 (d, 6H, J = 5), 2.209 (s, 6H); ^{13}C NMR (176 MHz, d^6-DMSO): 178.9587, 148.4411, 31.6750, 12.1330; MS: calcd for $CuC_8H_{15}N_6S_2$ [(M+H)$^+$] 322.01, found 322.08; for glyoxal-bis(4-methylthiosemicarbazone) (H_2GTSM), ^{1}H NMR (700 MHz, d^6-DMSO): 11.7317 (s, 2H), 8.4736 (q, 2H, J = 5, J = 13), 7.7182 (s, 2H), 2.9576 (d, 6H, J = 5); ^{13}C NMR (176 MHz, d^6-DMSO): 178.0312, 140.5007, 31.3725; MS: calcd for $CuC_6H_{11}N_6S_2$ [(M+H)$^+$] 293.90, found 294.00; for 1-phenyl-1,2-propanedione bis(4-methyl-3-thiosemicarbazone)[40] ($H_2\phi$MTSM), ^{1}H NMR (700 MHz, d6-DMSO): 10.704 (s, ^{1}H), 8.7402 (m, ^{1}H), 8.6505 (s, ^{1}H), 7.592−7.541 (m, 3H), 7.295−7.265 (m, 2H), 6.979 (m, ^{1}H), 3.043 (d, 3H, J = 5), 2.819 (d, 3H, J= 5), 2.373 (s, 3H); M.S.: calcd for $CuC_{13}H_{17}N_6S_2$ [(M + H$^+$)] 384.03, found 384.08. Cupric and zinc complexes were generally prepared as stock solutions obtained by adding a slight excess of a concentrated solution of $Cu(OAc)_2$ or $Zn(OAc)_2$ to the free ligand dissolved in DMSO; these were monitored spectrally using a Shimadzu UV-2041PC recording spectrophotometer to confirm complete formation of 1:1 complexes. During the course of subsequent experimentation, it was noted that the presence of even small amounts (∼2%) of DMSO partially inhibited release of Cu(II) (measured as formation of Cu^{II}PAR in experiments using peroxynitrite as oxidant). This protection almost certainly arose from scavenging of secondary peroxynitrite-derived oxidizing radicals by the DMSO. Additional experiments with peroxynitrite were therefore done using solid CuATSM that was solubilized in aqueous-based media devoid of DMSO; these studies indicated that the presence of DMSO at concentration levels present in the reaction medium caused only minor alteration of the reaction course. Solid CuATSM was obtained following a general procedure[41] that involved dropwise addition of aqueous $CuSO_4$ to a suspensions of H_2ATSM in methanol and isolating the CuATSM that precipitated. A more critical issue was the highly effective scavenging of HOCl by DMSO, which completely masked its reaction with CuATSM at even the millimolar concentration levels present following dilution of concentrated DMSO stock solutions of CuATSM into the reaction medium. This problem was circumvented by preparing CuATSM in *N*-methyl-2-pyrrolidone, which control studies showed did not reduce HOCl when diluted into the reaction medium for periods exceeding 1 h.

Myeloperoxidase (MPO) was isolated from bovine spleens by column chromatography as previously described;[42] the purified enzyme had an RZ value of 0.70 and a specific activity of 345 units/mg protein, as measured by the guaiacol assay.[43] Type VI horseradish peroxidase (HRP) was obtained from Sigma, and its activity was determined by HRP-catalyzed oxidation of 2,2′-azino-bis(3-ethylbenzothiazoline-6-sulfonic acid) (ABTS) with H_2O_2.[17]

Reactants. To investigate oxidative reactions, we used where possible aqueous buffered media containing 20−50 mM SDS. Under these conditions, most of the SDS is present as microphase-separated micelles. Specifically, the SDS critical micelle concentration is ∼8 mM, and its aggregation number in aqueous solutions is ∼60,[12] so that the effective concentration of micelles in these mixtures was 200−700 μM. Because the M^{II}(btsc) concentrations never exceeded 50 μM in these experiments, the average occupancy number, i.e., M^{II}(btsc)/micelle, was always less than 1. We believe that this medium effectively mimics the biological milieu inside eukaryotic cells, which contain numerous phase-separated microdomains.[13] Inclusion of SDS also serves to increase the effective solubility of the neutral Cu^{II}(btsc) complexes in aqueous media. As noted above, some of the reactions studied are incompatible with all system components. Most prominently, SDS inactivated the peroxidases (HRP, MPO) used in studying catalyzed oxidation by H_2O_2 and could not be included in the reaction medium. These studies utilized the Good's buffer, 3-(*N*-morpholino)propanesulfonic acid (MOPS), a neutral tertiary amine that does not strongly coordinate Cu(II). However, MOPS also protected CuATSM from reaction with peroxynitrite, so that it was necessary to substitute phosphate ion as the buffer component in reactions involving ONOOH and $ONOOCO_2^-$ as oxidants.

Reactant concentrations of free and metalated bis-thiosemicarbazones were determined spectrophotometrically in buffered aqueous/SDS micellar suspensions using independently measured molar absorptivities from serially diluted samples in the same medium. These standard solutions followed Beer's law over the entire concentration range encompassed in subsequent experiments. The extinction coefficients (in mM^{-1} cm^{-1}) at the peak maxima are as follows: H_2ATSM (ε_{326} = 45); CuATSM (ε_{309} = 21, ε_{465} = 5.6); ZnATSM (ε_{413} = 8.56); H_2GTSM (ε_{335} = ε_{346} = 41); CuGTSM (ε_{314}

DOI: 10.1021/acs.inorgchem.8b00853
Inorg. Chem. 2018, 57, 8923−8932

= 16.7, ε_{485} = 6.4); $H_2\phi$MTSM (ε_{333} = 45); CuϕMTSM (ε_{311} = 22, ε_{479} = 6.4); PAR (ε_{413} = 33); CuPAR (ε_{511} = 34). Reactant solutions of ONOOH were prepared by diluting into alkaline (pH > 12) water portions of frozen concentrated stocks (~0.1 M) that had been made by flow-mixing sodium nitrite with hydrogen peroxide;[44] concentrations were determined spectrophotometrically using ε_{302} = 1.67 mM^{-1} cm^{-1}.[45] Reactant solutions of hypochlorous acid were prepared by dilution of commercial bleach into H_2O and determining their concentrations spectrophotometrically in alkaline (pH > 12) solutions using $\varepsilon_{292}(OCl^-)$ = 350 M^{-1} cm^{-1}.[46] Reactant solutions of taurine chloramine were prepared by dropwise addition of HOCl to a final concentration of 10 mM into a rapidly stirred aqueous solution containing 2-fold excess taurine; spectrophotometric analysis confirmed the complete conversion of HOCl to the monochloramine without formation of detectable amounts of taurine dichloramine.

Instrumental Methods. Cyclic voltammograms were measured in DMSO with an EG&G Model 273 potentiostat/galvanostat using an electrochemical cell in a standard 3-electrode configuration with glassy carbon, Pt wire, and Ag/AgCl/KNO_3 working, counter and reference electrodes, respectively; 0.1 M tetrabutylammonium tetrafluoroborate was the inert electrolyte and ferrocene (Fc) was added internally as a reference standard to determine peak potentials. The $Fc^{+/o}$ potential in DMSO was taken to be 0.68 V vs NHE.[11] Sweep rates were typically 50 mV/s. Peroxidase-catalyzed oxidations of M^{II}(btsc) complexes were monitored spectroscopically by following the time course of bleaching of their optical bands using a Shimadzu UV-2041PC recording spectrophotometer interfaced to Shimadzu UVProbe software. This instrument was also used to make routine spectrophotometric analyses. Rapid reactions, including ONOOH and $ONOOCO_2^-$ decompositions, peroxynitrite oxidation of both M^{II}(btsc) complexes and PAR, and PAR complexation by Cu(II) were followed using an Applied Photophysics SX20 stopped-flow apparatus operated in the single-mixing absorption detection mode; kinetic traces were analyzed using the associated Pro-Data SX software. Transient spectra formed during reactions of CuATSM with peroxynitrite were recorded from 230 to 600 nm by using a Shimadzu Multispec 1500 instrument. Reactions were initiated by bolus addition of the peroxynitrite to buffered SDS micellar solutions containing CuATSM, followed by repetitive spectral determinations at 1−3 s intervals.

■ ASSOCIATED CONTENT

Supporting Information

The Supporting Information is available free of charge on the ACS Publications website at DOI: 10.1021/acs.inorgchem.8b00853.

Additional electrochemical, spectroscopic and kinetic information involving Cu^{II}(btsc) oxidations, Cu-PAR association dynamics, and ATSM inhibition of the HRP-catalyzed ABTS-H_2O_2 reaction (PDF)

■ AUTHOR INFORMATION

Corresponding Author

*E-mail: hurstja@onid.orst.edu.

ORCID

James K. Hurst: 0000-0003-1070-2690

Present Address

⊥J.J.S.: Department of Chemistry, Matanuska-Susitna College University of Alaska, Anchorage, Palmer, Alaska 99645, United States.

Notes

The authors declare no competing financial interest.

■ ACKNOWLEDGMENTS

This work was supported by the Office of the Assistant Secretary of Defense for Health Affairs through the Congressionally Directed Medical Research Program on ALS (AL140108, Award Number W81XWH-15-1-0289) and funding from the Oregon Chapter of the ALS Association (ALSA 16-320).

■ REFERENCES

(1) Vavere, A. L.; Lewis, J. S. Cu-ATSM: A Radiopharmaceutcal for the PET Imaging of Hypoxia. *Dalton Trans.* **2007**, 4893−4902.

(2) Crouch, P. J.; Hung, L. W.; Adlard, P. A.; Cortes, M.; Lal, V.; Filiz, G.; Perez, K. A.; Nurjono, M.; Caragounis, A.; Du, T.; Laughton, K.; Volitakis, I.; Bush, A. I.; Li, Q.; Masters, C. L.; Cappai, R.; Cherny, R. A.; Donnelly, P. S.; White, A. R.; Barnham, K. Increasing Cu Bioavailability Inhibits Aβ Oligomers and Tau Phosphorylation. *Proc. Natl. Acad. Sci. U. S. A.* **2009**, *106*, 381−386.

(3) Hung, L. W.; Villemagne, V. L.; Cheng, L.; Sherratt, N. A.; Ayton, S.; White, A. R.; Crouch, P. J.; Lim, S.; Leong, S. L.; Wilkins, S.; George, J.; Roberts, B. R.; Pham, C. L. L.; Liu, X.; Chiu, F. C. K.; Shackleford, D. M.; Powell, A. K.; Masters, C. L.; Bush, A. I.; O'Keefe, G.; Culvenor, J. G.; Cappai, R.; Cherny, R. A.; Donnelly, P. S.; Hill, A. F.; Finkelstein, D. I.; Barnham, K. J. The Hypoxia Imaging Agent Cu^{II}(atsm) is Neuroprotective and Improves Motor and Cognitive Functions in Multiple Animal Models of Parkinson's Disease. *J. Exp. Med.* **2012**, *209*, 837−854.

(4) Soon, C. P. W.; Donnelly, P. S.; Turner, B. J.; Hung, L. W.; Crouch, P. J.; Sherratt, N. A.; Tan, J.-L.; Lim, N. K-H.; Lam, L.; Bica, L.; Lim, S.; Hickey, J. L.; Morizzi, J.; Powell, A.; Finkelstein, D. I.; Culvenor, J. G.; Masters, C. L.; Duce, J.; White, A. R.; Barnham, K. J.; Li, Q.-X. Diacetylbis *N*(4)-methylthiosemicarbazonato) Copper(II) (Cu^{II}(atsm)) Protects against Peroxynitrite-induced Nitrosative Damage and Prolongs Survivial in Amyotrophic Lateral Sclerosis Mouse Model. *J. Biol. Chem.* **2011**, *286*, 44035−44044.

(5) Holland, J. P.; Giansiracusa, J. H.; Bell, S. G.; Wong, L.-L.; Dilworth, J. R. In vitro Kinetic Studies on the Mechanism of Oxygen-dependent Cellular Uptake of Copper Radiopharmaceuticals. *Phys. Med. Biol.* **2009**, *54*, 2103−2119.

(6) Fubayashi, Y.; Taniuchi, H.; Yoshihara, Y.; Ohtani, H.; Konishi, J.; Yokoyama, A. Copper-62-ATSM: A New Hypoxia Imaging Agent with High Membrane Permeability and Low Redox Potential. *J. Nucl. Med.* **1997**, *38*, 1155−1160.

(7) Obata, A.; Yoshimi, E.; Waki, A.; Lewis, J. S.; Oyama, N.; Welch, M. J.; Saji, H.; Yonekura, Y.; Fujibayashi, Y. Retention Mechanism of Hypoxia Selective Nuclear Imaging/Radiotherapeutic Agent Cu-diacetyl-bis(N^4-methylthiosemicarbazone) (Cu-ATSM) in Tumor Cells. *Ann. Nucl. Med.* **2001**, *15*, 499−504.

(8) Xiao, Z.; Donnelly, P. S.; Zimmermann, M.; Wedd, A. G. Transfer of Copper between Bis(thiosemicarbazone) Ligands and Intracellular Copper-Binding Proteins. Insights into Mechanisms of Copper Uptake and Hypoxia Selectivity. *Inorg. Chem.* **2008**, *47*, 4338−4347.

(9) Holland, J. P.; Barnard, P. J.; Collison, D.; Dilworth, J. R.; Edge, R.; Green, J. C.; McInnes, E. J. L. Spectroelectrochemical and Computational Studies on the Mechanism of Hypoxia Selectivity of Copper Radiopharmaceuticals. *Chem. - Eur. J.* **2008**, *14*, 5890−5907.

(10) McDonald, M. R.; Fredericks, F. C.; Margerum, D. W. Characterization of Copper(III)-Tetrapeptide Complexes with Histidine as the Third Residue. *Inorg. Chem.* **1997**, *36*, 3119−3124. Hanss, J.; Beckmann, A.; Krüger, H.-J. Stabilization of Copper(III) Ions with Deprotonated Hydroxyiminoamide Ligands: Syntheses, Structures, and Electronic Properties of Copper(II) and Copper(III) Complexes. *Eur. J. Inorg. Chem.* **1999**, *1999*, 163−172. Fritsky, I. O.; Kozlowski, H.; Kanderal, O. M.; Haukka, M.; Swiatek-Kozlowska, J.; Gumienna-Kontecka, E.; Meyer, F. Efficient Stabilization of Copper-(III) in Tetraaza Pseudo-macrocyclic Oxime- and Hydrazide Ligands with Adjustable Cavity Size. *Chem. Commun.* **2006**, 4125−4127. Pratesi, A.; Zanello, P.; Giorgi, G.; Messori, L.; Laschi, F.; Casini, A.;

DOI: 10.1021/acs.inorgchem.8b00853
Inorg. Chem. 2018, 57, 8923−8932

Corsini, M.; Gabbiani, C.; Orfei, M.; Rosani, C.; Ginanneschi, M. New Copper(II)/Cyclic Tetrapeptide System that Easily Oxidizes to Copper(III) under Atmospheric Oxygen. *Inorg. Chem.* **2007**, *46*, 10038−10040. Keown, W.; Gary, J. B.; Stack, T. D. P. High-valent Copper in Biomimetic and Biological Oxidations. *JBIC, J. Biol. Inorg. Chem.* **2017**, *22*, 289−305.

(11) Barrette, W. C., Jr.; Johnson, H. W.; Sawyer, D. T. Voltammetric Evaluation of the Effective Acidities (pKa') for Broensted Acids in Aprotic Solvents. *Anal. Chem.* **1984**, *56*, 1890−1898.

(12) Dominguez, A.; Fernández, A.; González, N.; Iglesias, E.; Montenegro, L. Determination of the Critical Micelle Concentration of Some Surfactants by Three Techniques. *J. Chem. Educ.* **1997**, *74*, 1227−1231.

(13) Hickey, J. L.; James, J. L.; Henderson, C. A.; Price, K. A.; Mot, A. I.; Buncic, G.; Crouch, P. J.; White, J. M.; White, A. R.; Smith, T. A.; Donnelly, P. S. Intracellular Distribution of Fluorescent Copper and Zinc Bis(thiosemicarbazonato) Complexes Measured with Fluorescence Lifetime Spectroscopy. *Inorg. Chem.* **2015**, *54*, 9556−9567.

(14) Furtmüller, P. G.; Arnhold, J.; Jantschko, W.; Pichler, H.; Obinger, C. Redox Properties of the Couples Compound I/Compound II and Compound II/Native Enzyme of Human Myeloperoxidase. *Biochem. Biophys. Res. Commun.* **2003**, *301*, 551−557.

(15) Hayashi, Y.; Yamazaki, I. The Oxidation-Reduction Potentials of Compound I/Compound II and Compound II/Ferric Couples in Horseradish Peroxidases A_2 and C. *J. Biol. Chem.* **1979**, *254*, 9101−9106.

(16) Ooi, S.; Carter, D.; Fernando, Q. The Structure of a Chelate of Copper(II) with 1-(2-Pyridylazo)-2-Napthol. *Chem. Commun.* **1967**, 1301−1302.

(17) Childs, R. E.; Bardsley, W. G. The Steady-state Kinetics of Peroxidase with 2,2′-Azino-di-(3-ethyl-benzthiazoline-6-sulphonic acid) as Chromagen. *Biochem. J.* **1975**, *145*, 93−103.

(18) Klebanoff, S. J.; Kettle, A.; Rosen, H.; Winterbourn, C. C.; Nauseef, W. M. Myeloperoxidase: A Front-line Defender Against Phagocytosed Microorganisms. *J. Leukocyte Biol.* **2013**, *93*, 1−14. Hurst, J. K. What Really Happens in the Neutrophil Phagosome? *Free Radical Biol. Med.* **2012**, *53*, 508−520.

(19) Pacher, P.; Beckman, J. S.; Liaudet, L. Nitric Oxide and Peroxynitrite in Health and Disease. *Physiol. Rev.* **2007**, *87*, 315−424.

(20) Ischiropoulos, H.; Zhu, L.; Beckman, J. S. Peroxynitrite Formation from Macrophage-derived Nitric Oxide. *Arch. Biochem. Biophys.* **1992**, *298*, 446−451.

(21) Lymar, S. V.; Hurst, J. K. Rapid Reaction between Peroxonitrite Ion and Carbon Dioxide: Implications for Biological Reactivity. *J. Am. Chem. Soc.* **1995**, *117*, 8867−8868.

(22) Coddington, J. S.; Hurst, J. K.; Lymar, S. V. Hydroxyl Radical Formation during Peroxynitrous Acid Decomposition. *J. Am. Chem. Soc.* **1999**, *121*, 2438−2444.

(23) Goldstein, S.; Lind, J.; Merényi, G. Chemistry of Peroxynitrites as Compared to Peroxynitrates. *Chem. Rev.* **2005**, *105*, 2457−2470.

(24) Stanbury, D. A. Reduction Potentials involving Inorganic Radicals in Aqueous Solution. *Adv. Inorg. Chem.* **1989**, *33*, 69−138.

(25) Ferrer-Sueta, G.; Campolo, N.; Trujillo, M.; Bartesaghi, S.; Carballal, S.; Romero, N.; Alvarez, B.; Radi, R. Biochemistry of Peroxynitrite and Protein Tyrosine Nitration. *Chem. Rev.* **2018**, *118*, 1338−1408.

(26) Jazdzewski, B. A.; Tolman, W. B. Understanding the Copper-Phenoxyl Radical Array in Galactose Oxidase: Contributions from Synthetic Modeling Studies. *Coord. Chem. Rev.* **2000**, *200−202*, 633−685.

(27) Roy, N.; Sproules, S.; Weyhermüller; Wieghardt, K. Trivalent Iron and Ruthenium Complexes with a Redox Noninnocent (2-Mercaptophenylimino)-methyl-4,6-di-tert-butylphenolate(2-) Ligand. *Inorg. Chem.* **2009**, *48*, 3783−3791.

(28) Neishi, H.; Ikawa, M.; Okazawa, H.; Tsujikawa, T.; Arishima, H.; Kikuta, K. I.; Yoneda, M. Precise Evaluation of Striatal Oxidative Stress Corrected for Severity of Dopaminergic Neural Degeneration in Patientis with Parkinson's Disease: A Study with ^{62}Cu-ATSM PET and ^{123}I-FP-CIT SPECT. *Eur. Neurol.* **2017**, *78*, 161−168.

(29) Donnelly, P. S.; Liddell, J. R.; Lim, S.-C.; Paterson, B. M.; Cater, M. A.; Savva, M. S.; Mot, A. I.; James, J. L.; Trounce, I. A.; White, A. R.; Crouch, P. J. An Impaired Mitochondrial Electron Transport Chain Increases Retention of the Hypoxia Imaging Agent Diacetylbis(4-methylthiosemicarbazonato)copper^{II}. *Proc. Natl. Acad. Sci. U. S. A.* **2012**, *109*, 47−52.

(30) Stefani, C.; Al-Eisawi, Z.; Jansson, P. J.; Kalinowski, D. S.; Richardson, D. R. Identification of Differential Anti-neoplastic Activity of Copper bis(thiosemicarbazones) that is Mediated by Intracellular Reactive Oxygen Species Generation and Lysosomal Membrane Permeation. *J. Inorg. Biochem.* **2015**, *152*, 20−37.

(31) Whittaker, J. W. The Free Radical-Coupled Copper Oxidative Site in Galactose Oxidase. In *Metal Ions in Biological Systems*; Sigel, H., Sigel, A., Eds.; Marcel Dekker: New York, 1994; Vol. *30*, pp 315−360.

(32) Chaudhuri, P.; Hess, M.; Müller, J.; Hildenbrand, K.; Bill, E.; Weyhermüller, T.; Wieghardt, K. Aerobic Oxidation of Primary Alcohols (Including Methanol) by Copper(II)- and Zinc(II)-Phenoxyl Radical Catalysts. *J. Am. Chem. Soc.* **1999**, *121*, 9599−9610.

(33) Choi, D.-K.; Pennathur, S.; Perier, C.; Tieu, K.; Teismann, P.; Wu, D.-C.; Jackson-Lewis, V.; Vila, M.; Vonsattel, J.-P.; Heinecke, J. W.; Przedborski, S. J. Ablation of the Inflammatory Enzyme Myeloperoxidase Mitigates Features of Parkinson's Disease in Mice. *Neuroscience* **2005**, *25*, 6594−6600.

(34) Maki, R. A.; Tyurin, V. A.; Lyon, R. C.; Hamilton, R. L.; DeKosky, S. T.; Kagan, V. E.; Reynolds, W. F. Aberrant Expression of Myeloperoxidase in Astrocytes Promotes Phospholipid Oxidation and Memory Deficits in a Mouse Model of Alzheimer Disease. *J. Biol. Chem.* **2009**, *284*, 3158−3169.

(35) Green, P. S.; Mendez, A. J.; Jacob, J. S.; Crowley, J. R.; Growdon, W.; Hyman, B. T.; Heinecke, J. W. Neuronal Expression of Myeloperoxidase is Increased in Alzheimer's Disease. *J. Neurochem.* **2004**, *90*, 724−733.

(36) Jeitner, T. M.; Kalogiannis, M.; Krasnikov, B. F.; Gomlin, I.; Peltier, M. R.; Moran, G. R. Linking Inflammation and Parkinson Disease: Hypochlorous Acid Generates Parkinsonian Poisons. *Toxicol. Sci.* **2016**, *151*, 388−402.

(37) Elzanowska, H.; Wolcott, R. G.; Hannum, D. M.; Hurst, J. K. Bactericidal Properties of Hydrogen Peroxide and Copper or Iron-containing Complex Ions in Relation to Leukocyte Function. *Free Radical Biol. Med.* **1995**, *18*, 437−449.

(38) Djoko, K. Y.; Paterson, B. M.; Donnelly, P. S.; McEwan, A. G. Antimicrobial Effects of Copper(II) Bis(thiosemicarbazonato) Complexes Provide New Insight into their Biochemical Mode of Action. *Metallomics* **2014**, *6*, 854−863.

(39) Djoko, K. Y.; Goytia, M. M.; Donnelly, P. S.; Schembri, M. A.; Shafer, W. M.; McEwan, A. G. Copper(II)-Bis(Thiosemicarbazonato) Complexes as Antibacterial Agents: Insights into Their Mode of Action and Potential as Therapeutics. *Antimicrob. Agents Chemother.* **2015**, *59*, 6444−6453.

(40) Beraldo, H.; Kaisner, S. B.; Turner, J. D.; Billeh, I. S.; Ives, J. S.; West, D. X. Copper (II) and Nickel(II) Complexes of the Bis{N(3)-Substituted Thiosemicarbazones} of Phenylglyoxyl and 1-Phenyl-propane-1,2-Dione. *Transition Met. Chem.* **1997**, *22*, 459−464.

(41) Hueting, R.; Christlieb, M.; Dilworth, J. R.; Garayoa, E. G.; Gouverneur, V.; Jones, M. W.; Maes, V.; Schibli, R.; Sun, X.; Tourwé, D. Bis(thiosemicarbazones) as bifunctional chelators for the room temperature 64-copper labeling of peptides. *Dalton Trans.* **2010**, *39*, 3620−3632.

(42) Ikeda-Saito, M. Spectroscopic, Ligand Binding, and Enzymatic Properties of Spleen Green Hemeprotein. A Comparison with Myeloperoxidase. *J. Biol. Chem.* **1985**, *260*, 11688−11695.

(43) Klebanoff, S. J.; Waltersdorph, A. M.; Rosen, H. Antimicrobial Activity of Myeloperoxidase. *Methods Enzymol.* **1984**, *105*, 399−403.

(44) Saha, A.; Goldstein, S.; Cabelli, D.; Czapski, G. Determination of Optimal Conditions for Synthesis of Peroxynitrite by Mixing

DOI: 10.1021/acs.inorgchem.8b00853
Inorg. Chem. 2018, 57, 8923−8932

Hydrogen Peroxide with Nitrite. *Free Radical Biol. Med.* **1998**, *24*, 653−659.
(45) Hughes, M. N.; Nicklin, H. G. The Chemistry of Pernitrites. Part I. Kinetics of Decomposition of Pernitrous Acid. *J. Chem. Soc. A* **1968**, 450−452.
(46) Morris, J. C. The acid ionization constant of HOCl from 5 to 35 °C. *J. Phys. Chem.* **1966**, *70*, 3798−3805.

DOI: 10.1021/acs.inorgchem.8b00853
Inorg. Chem. 2018, 57, 8923−8932